Colloidal Superstructures Programmed into Magnetic Janus Particles

*Jing Yan, Sung Chul Bae, and Steve Granick**

Magnetic interaction has long been used to generate responsive colloidal superstructures, the classical example being ferrofluids.[1] The more recent availability of monodisperse, superparamagnetic colloids with embedded magnetic nanoparticles allows the preparation of regular periodic structures with optical properties suitable for photonic applications.[2] Moreover, going beyond the simple case of static magnetic fields, time-dependent magnetic fields, especially biaxial (rotating) and triaxial (precessing) have been shown to give rise to self-assembled structures with unusual symmetry and anisotropic magnetic, electrical, and thermal responses not achievable using a uniaxial field.[3,4] Using multiaxial fields allows greater freedom in selecting magnetic structures by introducing extra parameters such as frequency and relative strength between the field intensity in various directions.[5] Moreover, time-dependent fields have the potential to introduce dynamics into the individual building blocks, producing a new variety of advanced material.[6] Studies to date, however, mainly employed homogeneous particles such that their magnetic properties can be represented as dipolar spheres and this limits the possible crystal lattices into which they can assemble.[7] To expand the possibilities calls for more sophisticated engineering of the colloidal units. The recent surge of interest in anisotropic building blocks has inspired us to design new magnetic colloids for this purpose.[8]

The novelty of this paper is to show that thin-film engineering of magnetic coatings onto spherical colloid-sized particles (**Figure 1**a) can produce a rich and diverse variety of new, programmable structures in a homogeneous rotating magnetic field. The simplicity of the particle design and synthesis introduced here is generalizable. The main idea is to capitalize upon the monodisperse spheres that in colloid science have been widely accessible,[9] and using thin-film engineering to endow them with magnetic responsiveness. The proof-of-concept presented here is shown for the simplest departure from the prototypical dipolar spheres: magnetic Janus spheres.[10,11] Previously, this lab employed precessing magnetic fields to produce synchronized rotating microtubules from simple magnetic Janus spheres,[10] and demonstrated the effect of shape anisotropy in zero-field assembly.[12] In this paper, we delve deeper into the thin-film properties and, in combination with manipulation of the magnetic field strength and frequency, demonstrate exquisite control over properties of the building blocks and their subsequent self-assembly structures.

We set out first to synthesize and understand the magnetic property of single Janus spheres. Using electron beam deposition, we sequentially deposited a trilayer sandwich of 2 nm Ag/5–30 nm Ni/15 nm SiO_2 onto commercially obtained spherical silica particles in the size range of 2–3 μm, whose advantage is that in subsequent studies their superstructures are readily viewed in an optical microscope. The selected range of Ni thickness was optimized to give minimal uncontrolled aggregation yet robust response to magnetic fields. In designing the trilayer, the Ag layer was used as a seed layer to improve the quality of the nickel film, and the thin silica outer shell was used to protect the magnetic material against oxidation, reduce the van der Waals attraction between metals, and to render the particles chemically isotropic on both hemispheres. This laboratory showed recently that the design is easily generalized to particles of other shapes.[12] As other potential choices of magnetic material exist,[13] there is broad potential to custom-tailor magnetic properties of colloids using this approach.

A curved film complicates its magnetic properties, however. If a film is planar, shape anisotropy pins the magnetic moment almost exclusively in the plane; but on a sphere, the surface normal changes continuously.[14] Therefore, for a curved film, both the out-of-plane and in-plane responses are a mixture of the parallel- and perpendicular-response that one measures in a flat film of the same metal, shown by the hysteresis curve that we measured (Figure 1b). The larger dimension in the parallel direction of the coating (approximately particle diameter) than in the perpendicular direction (approximately particle radius) promotes predominant magnetic response parallel to the Janus interface. Moreover, the pinch-off of the hysteresis curve in the direction parallel to the Janus interface indicates a magnetic vortex state (Figure 1b (inset)): rather than coherent rotation of magnetic spins, a magnetic vortex nucleates on the hemispherical cap of Janus particles, when the direction of the magnetic field is reversed.[15]

The second consequence of directional deposition onto spheres is uneven distribution of magnetic material: the film is thickest at the apex of the sphere and tapers toward the equator, following a cosine relationship with respect to the zenith angle.[16] The effect of the directional coating can be modeled by a magnetic dipole shifted from the object's geometric center, which depends on the coating thickness (Figure 1a).[17] This dipole offset causes particles to form zigzag chains in a static field, with a zigzag angle θ. We have measured θ for different nominal coating thickness t_{Ni} and observed a monotonic trend: the thicker the coating, the larger the angle θ (Figure 1c). As shown in Figure 1d, a larger

Dr. J. Yan, Prof. S. Granick
Departments of Materials Science and Engineering
Chemistry and Physics
University of Illinois at Urbana-Champaign
1304 W. Green St., Urbana, Illinois 61801, USA
E-mail: sgranick@illinois.edu
Prof. S. C. Bae
Department of Biomedical Engineering
Ulsan National Institute of Science and Technology
UNIST-gil 50, Ulju-gun, Ulsan 689–798, South Korea

DOI: 10.1002/adma.201403857

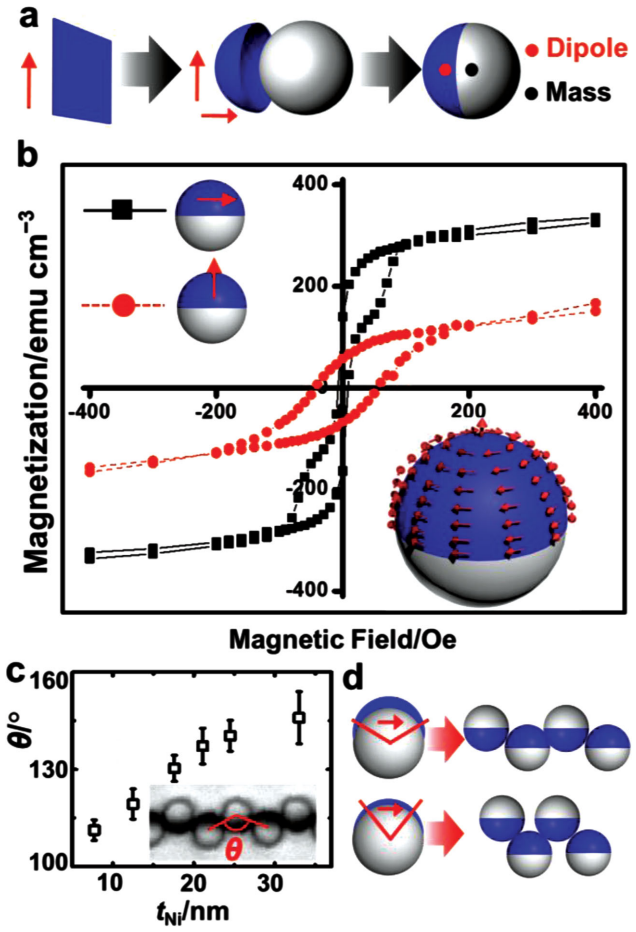

Figure 1. Individual particles. a) Schematic representation of the particle design. The hemispherical magnetic thin film cap acquires magnetic response in two orthogonal directions (red arrows) with dipole moment (red spot) offset from the center of mass (black spot). b) Magnetic hysteresis curve of a dense monolayer of Janus particles ($d = 2$ μm, $t_{Ni} = 18$ nm) with direction of measurement indicated in the inset. The pinch-off of the hysteresis curve indicates a magnetic vortex state in the hemispherical cap, shown in the bottom right inset. c) Zigzag angle θ versus t_{Ni}. Inset shows a typical zigzag chain in static field with definition of angle θ. All θs are measured for chains assembled in a static 5 mT field with $d = 3$ μm. d) Schematic representation of the relationship between t_{Ni}, dipole offset, and θ. The red angle defines the region that contributes to the magnetic moment. Thinner coatings have smaller effective surface area, giving larger offset and hence smaller θ.

zigzag angle signifies smaller dipole offset. To understand this, note that the magnetization of Ni films is reduced at thickness below ≈4 nm because the films cease to be continuous,[18] and moreover on a porous SiO_2 substrate, this threshold thickness is expected to be even larger. Therefore, only the middle region of the film with sufficient thickness contributes to the magnetic response, and this effective region leans toward the edge of the particle, away from the particle center. Hence, the thinner the film, the smaller the effective magnetic region, and the larger the dipole offset. To experimentalists, this provides extra control to fine-tune interparticle interaction, which depends on the dipole offset. The measurement of θ gives a convenient way to access the extent of dipole shift, and this approach has been proved to give satisfactory results.[10]

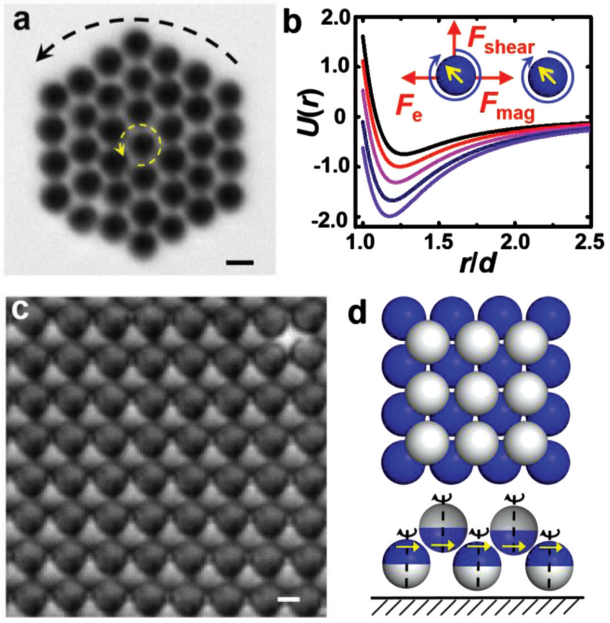

Figure 2. 2D assembly of Janus particles in rotating magnetic field. a) A piece of hexagonally ordered crystal in a rotating B field (20 Hz, 2 mT). The small yellow arrow indicates particle rotation. The large black arrow indicates rotation of the entire crystal piece. b) Pair potential $U(r)$ in unit of 10^{-18} J, calculated from $U(r) = -\mu_0 m^2 / 8\pi r^3 + 2\pi\varepsilon\varepsilon_0\zeta^2 R\ln[1+\exp(-\kappa(r-d))]$, in which ε is the dielectric constant of water (79.8 at 294 K), ε_0 is the vacuum permittivity, μ_0 is the vacuum permeability, m is the magnetic dipole strength, ζ is the particles' zeta potential (–34 ± 6 mV), and κ^{-1} is the Debye length (≈160 nm). Interparticle distance r is normalized by particle diameter d. From top to bottom, the curves correspond to pair potentials in external fields of 1, 2, 4, 10, and 20 mT. Inset: Relevant forces: electrostatic repulsion F_e, time-averaged magnetic attraction F_{mag}, and hydrodynamic shear force F_{shear}. c) Snapshot of a small region of crystal with square symmetry, formed by particles ($d = 3$ μm and $t_{Ni} = 7.6$ nm) in a 5 mT, 20 Hz rotating field. The imaging focus plane is on the bottom particle layer. The bottom layer particles appear as opaque spheres whereas the top layer particles appear as brighter spots in-between. d) Schematic illustrations of the structure shown in c), as viewed from the top (top) and from the side (bottom). Scale bars: 2 μm.

Next, we explore the self-assembly behavior of these Janus magnets in a rotating magnetic field of moderate strength (2–5 mT). In this strength range, the magnetic cap responds by shifting the center of the vortex and has almost linear magnetic response. In water suspension, these silica Janus spheres sediment to the chamber bottom due to density mismatch. Meanwhile, the much larger magnetic response in the transverse direction ensures that the particle aligns instantly with the Janus interface parallel to the external field. For most values of coating thickness, extended hexagonal crystals result (**Figure 2**a and Movie S1, Supporting Information). In this crystalline state, all particles appear opaque in optical images; their metal caps point perpendicular to the rotating field, uniformly in the same direction to minimize the dipole–dipole distance, and block light.

Close inspection shows that within these hexagonal crystals, the Janus sphere elements rotate synchronously with the external field. Therefore, the relative orientation of the instantaneous dipole moments of two neighboring

particles is well-defined, leading to a time averaged attraction $U(r)_{attr} = -\mu_0 m^2 / 8\pi r^3$, in which r is the dipoles' center-to-center distance and m is the dipole strength.[4] Balancing this with electrostatic repulsion,[19] we arrived at the effective pair potential shown in Figure 2b. The predicted minimum at around $1.2d$ agrees well with the interparticle distance that we measured (2.47 ± 0.02 μm for Figure 2a). Moreover, the position of the minimum is easily shifted by changing the external field strength. Such layering of rotating magnetic particles has long been predicted by computer simulation and recently confirmed by this lab.[20] A feature not predicted by simulation is that the crystal piece also rotates as a whole, with a much smaller angular velocity (≈1.6 Hz for this cluster). A simple physical argument explains this. In a pair of spinning colloids in close proximity, each exerts hydrodynamic shear force on the other.[21] The total shear force vanishes for a particle surrounded symmetrically by neighbors, but at the boundary it does not vanish. This is why the entire cluster experiences an effective shear at its boundary, resulting in cluster rotation. Similar cluster rotation is also seen for isotropic, paramagnetic spheres, but at much lower speed due to a completely different origin.[22]

Moving out of strictly 2D films where the expected symmetry is hexagonal, magnetic interactions become more complex. Janus spheres may distribute into different heights to reduce the dipole–dipole separation, as magnetic interactions (≈10^3 k_BT) dominate gravitational energy (≈10 k_BT). This requires large dipole offset. Indeed, for the smallest coating thickness (t_{Ni} = 7.6 nm), we observed a transition to a new lattice type (Figure 2c) in which particles split into two parallel planes pointing in opposite directions (Figure 2d). Meanwhile, minimization of interplane interactions transforms the lattice symmetry in each plane to square. Stacking additional planes could potentially lead to 3D body-centered-tetragonal lattices with alternating magnetic layers in the vertical (c) direction.[23]

Next, we systematically examine the effect of the field strength. Surprisingly, upon raising the magnetic field (≈30 mT), we observed an unexpected transition: single particles "grab" each other and face their magnetic hemispheres inward to form a dumbbell. Within the hexagonal crystals of single particles (**Figure 3** and Movie S2, Supporting Information), particles first vibrate vigorously in the lattice upon increasing the field strength, and when they come close to contact they link (Figure 3d). These dicolloids are slightly asymmetric, one particle pointing slightly off-axis. Conversion is instantaneous and almost complete, consuming almost all of the monomers. Once formed, each dicolloid starts to rotate around its own center of mass, which protects it from further aggregation. Note that such dicolloids have a different configuration from the staggered configuration of two particles in static field. Moreover, they align their long axis parallel to the

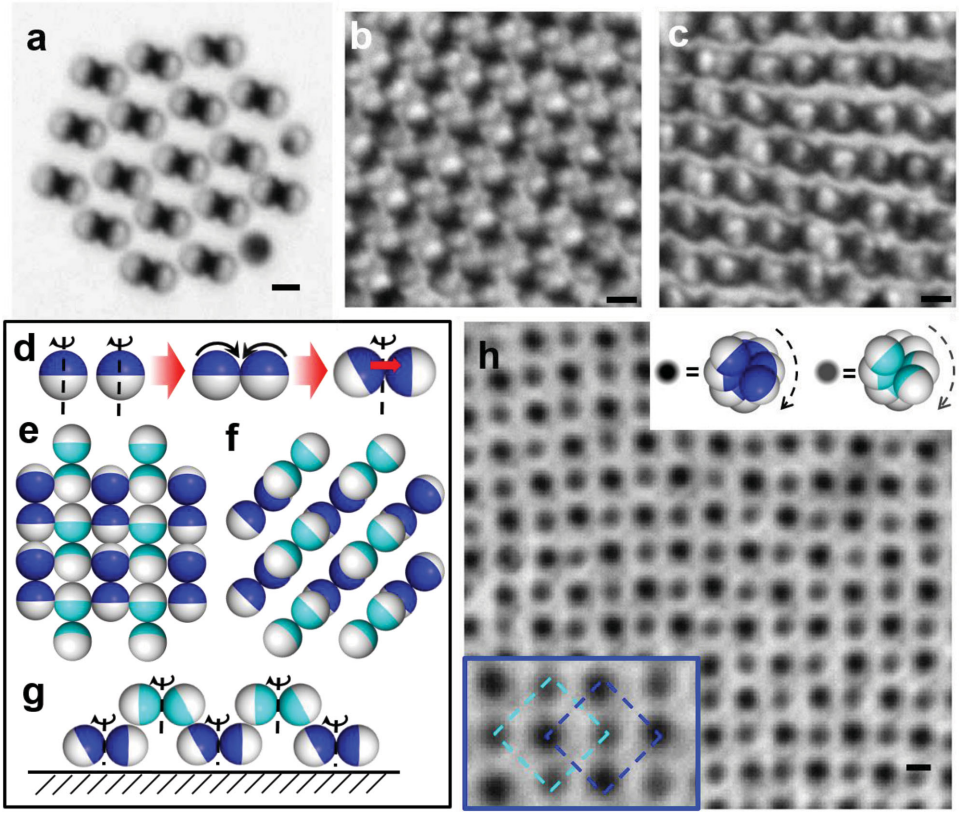

Figure 3. Colloidal crystals of dicolloids in rotating magnetic fields. a) Snapshot of a 2D cluster. b,c) Snapshots of a square dicolloid array inside a large rotating aggregate. d) Schematics of the dicolloid formation process. e,f) Top view of dicolloid arrangement in b) and c). g) Side view of dicolloid arrangement in (c). h) Long exposure optical image. Top right inset: the darker spots correspond to rotating dicolloids in the focal plane (blue in the cartoon). The grey spots correspond to dicolloids in a second plane (cyan in the cartoon). Bottom left inset: enlarged view of small area of the lattice. Scale bars: 2 μm.

external field (see below), contrary to what would be expected from single particle response. This transition also occurs in static field at a similar threshold of magnetic field; the advantage of a rotating field is to spatially concentrate the particles to generate many binary collision events in a short time. In other words, the initial hexagonal crystal provides an optimal reaction vessel for the formation of dicolloids.

We favor the following mechanism for dicolloid formation, although it is speculative. As the magnetic field is high, the interparticle distance experiences large changes during each cycle of particle rotation, so behavior time-averaged over the full cycle is no longer relevant. Instantaneously, it seems that particles experience strong attraction that drives them into close contact. As a common scenario in colloidal science, van der Waals attraction holds the particles together irreversibly when they come into physical contact.[24] Once this happens, the rotating field is not able to shear the two particles apart; they move as a whole. However, the orientation of the particles in the dimer is not fully understood. At high field strengths, the magnetic cap experiences almost full magnetization; the vortex core is expelled from the cap. Neighboring particles tend to point towards each other to concentrate their magnetic elements, although discrete particles still prefer to align parallel to the external field due to having larger moment in that configuration. The observed off-axis configuration of these dicolloid particles may represent a compromise between these two competing trends. Finite element analysis might, in the future, be employed to understand this point in further detail. The main point of our observation is that once formed, the dumbbell structures are stable, and their behavior is the same regardless of magnetic field strength.

With these new building blocks in hand, we start again to explore their assembly behavior in rotating magnetic fields. Small clusters of dicolloids retain hexagonal symmetry, with lattice constant twice as large as that for single particles (Figure 3a and Movie S3, Supporting Information). While the dumbbell shape breaks spherical symmetry instantaneously, rotation restores spherical symmetry such that the centers of the dicolloids again form a hexagonal lattice. This is also robust to the presence of small numbers of residual monomers.

Larger, denser aggregates are more complex. Figure 3b,c shows two snapshots of such aggregates (see also Movie S4, Supporting Information). In Figure 3b, the lobes of the dicolloids pack closely as squares, as schematically shown in Figure 3e. After $\pi/4$ rotation, the lobes appear to overlap but this is physically impossible, and in fact they have separated into different 2D planes. To show this, we used long camera exposure time to average out the angular information and focused on the center of mass arrangement. In Figure 3h, in addition to square symmetry, one sees two species with different intensities. Each forms a square array and they penetrate to form a superlattice in this 2D projection. The darker points correspond to the dicolloids within the focus plane, the lighter points to the plane that is stacked above (below) it, and their relative intensity could be reversed by changing the camera focus. Therefore, the following arrangement is proposed for the observed assembly: within each plane, dicolloids are arranged in a square lattice with center-to-center distance about $2d$, but within an adjoining plane, other dicolloids with the same arrangement are separated by a vertical distance $\approx 0.91d$ (see Figure S2, Supporting Information for geometric calculation) and shifted by half of the lattice constant in both x- and y-axes (Figure 3e–g). Tracking the projected inter-dicolloid distance gives the value of $1.46d$, close to the $\sqrt{2}d$ predicted by the proposed structure. This square superlattice is a direct result of dicolloids' dipole being offset from their center, which in turn results from asymmetry of the dicolloid configuration.

A vivid demonstration of the consequence of dipole offset is the assembly of dicolloids in static magnetic field (**Figure 4**a): they arrange into a staggered chain that looks like a footstep, not into the head-to-tail configuration expected for point dipoles. Closer inspection shows that the tilted monomer points

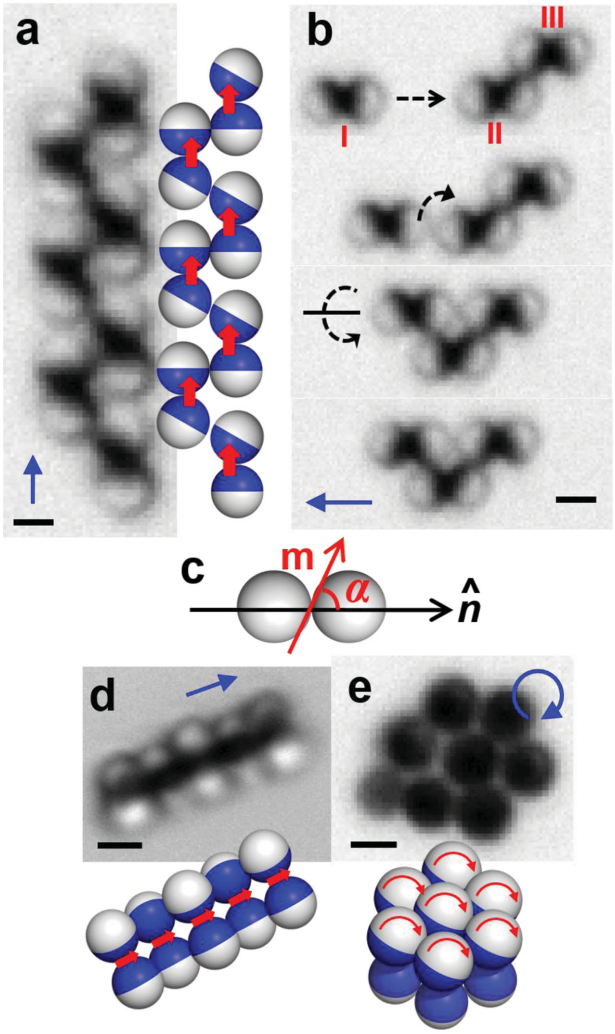

Figure 4. Assemblies of isomeric dicolloids. a) Footstep assembly in static magnetic field and its schematic representation. b) Snapshots of incorporation of a dicolloid into an existing footstep-chain. From top to bottom: t = 0, 355, 1065, 1420 ms. c) Schematics showing possible arrangement of dicolloid director $\hat{n}$ and dipole moment **m**, and the angle α between the two. d) Centipede assembly with $\alpha = 90°$ in a static magnetic field and its schematic representation. e) Hexagonal magnetic bilayer of dicolloids rotating around their long axis and corresponding schematic representation. The grey particle is a residual monomer. Scale bars: 2 μm. The blue arrows indicate the direction of the magnetic fields.

towards the centerline, reminiscent of single particle behavior. Relative to the head-to-tail configuration of single particles, in this staggered configuration the distance between dipoles is shorter. The kinetics of chain formation is consistent with this interpretation. In Figure 4b and Movie S5, Supporting Information, one sees the following sequence. First, an incoming dicolloid I is attracted by the long-range dipolar field to form a head-to-tail configuration with dicolloid II. Once in close contact with II, it further minimizes energy by sliding along II's contour to a new position where it interacts favorably with two dicolloids, II and III. Finally, it rotates around its long axis and positions its dipole closer to the centerline, which maximizes dipolar attraction.

The orthogonal anisotropy of the dipole and shape in such dicolloids leads us to hypothesize that the dipole moment could possess any angle α with respect to the dicolloid's long axis (Figure 4c), each α giving a different building block. When subjected to a fast oscillating field of 20 Hz, the dicolloid with $\alpha = 0°$ cannot follow the field and ends up with its short axis aligned with the AC field such that gradually it becomes magnetized along this short axis. This process, in effect, transforms the dicolloid from $\alpha = 0°$ to $\alpha = 90°$. The new isomeric dicolloids then attract side by side and form a centipede-like chain (Figure 4d) in a static field, consistent with dumbbells having a moment along the short axis.[25] When subjected to a rotating field, they stand vertically and rotate around their long axis as if in a ballet pirouette (Figure 4e), rather than spin in the plane, as the former presents less viscous drag. Meanwhile, they attract one another much as monomers do, forming a hexagonally close packed bilayer (Movie S6, Supporting Information). This isomerization phenomenon, demonstrated here for the specific case of two types of dicolloids, can be generalized to any anisotropic particle with more than two degrees of anisotropy.

In summary, simple magnetic Janus spheres have been shown to generate a rich variety of colloidal superstructures that present novel crystalline symmetry. The simple approach of engineering, the size of the spheres, and the magnetic coating thickness afford precise control of magnetic properties, especially the anisotropic susceptibility and dipole offset, which govern global symmetry changes when the particles are assembled. By driving the magnetic field into a regime of nonlinear response, we observe a drastic transition in the building block such that spheres pair into dicolloids that subsequently assemble into a plethora of new structures due to the peculiar properties of the dicolloids. This study points to a fruitful direction in designing new kinds of reconfigurable colloidal superstructures based on more complex particle shapes known in the field of colloids but not yet united with magnetic thin films, thus allowing huge design freedom in engineering magnetic building blocks.[26] The 2D nature of the metal deposition synthesis limits the scalability of this method at this moment; but with advances in the mass production of colloidal monolayers,[27] one could potentially obtain large amounts of such Janus particles, and other methods are also imaginable by rational extrapolation.[28] The tunable nature of their assembly makes them potential candidates for responsive materials, especially when the anisotropic structures would be frozen into place with known methods.[29,30]

Experimental Section

The magnetic Janus particles were synthesized using electron beam deposition onto silica particles (Tokuyama) either 2 or 3 μm in diameter, following a reported procedure.[9] The film thickness was measured by ellipsometry (J. A. Woollam VASE ellipsometer), with a control glass slide coated at the same time of the particle synthesis. Before being sonicated off the glass slides, the particles were magnetized in the film direction. The details of the magnetic and imaging setup have been reported elsewhere.[9] Briefly, a homogeneous rotating magnetic field (up to 50 mT) was generated by applying two sinusoidal signals with a $\pi/2$ shift to two pairs of iron-core solenoids placed at an orthogonal angle, using either a function generator or Labview controlled I/O board. The AC signals were amplified with a dual channel power amplifier (Crown, XLS 202). A static magnetic field was generated by attaching one pair of solenoids to a DC power supply. Hysteresis loop measurements were carried out using a Quantum Design SQUID magnetometer MPMS-XL. The zeta potential was measured using a Malvern Zetasizer Nano. The Debye length was inferred from conductivity measurements made immediately before the experiment, following a standard procedure.[31]

Supporting Information

Supporting Information is available from the Wiley Online Library or from the author.

Acknowledgements

This work was supported by the US Department of Energy, Division of Materials Science, under the Award No. DE-FG02–07ER46471 through the Frederick Seitz Materials Research Laboratory at the University of Illinois at Urbana-Champaign.

Received: August 22, 2014
Revised: October 24, 2014
Published online: December 12, 2014

[1] R. E. Rosensweig, *Ferrohydrodynamics*, Dover, Mineola, NY, USA **1997**.
[2] a) J. Ge, Y. Yin, *Adv. Mater.* **2008**, *20*, 3485; b) M. Wang, L. He, Y. Yin, *Mater. Today* **2013**, *16*, 110.
[3] a) D. H. Read, J. E. Martin, *Adv. Funct. Mater.* **2010**, *20*, 1577; b) J. E. Martin, *Composites, Part A* **2005**, *36*, 545; c) D. Du, D. Li, M. Thakur, S. L. Biswal, *Soft Matter* **2013**, *9*, 6867; d) J. Ćernák, G. Helgesen, *Phys. Rev. E* **2008**, *78*, 061401; e) G. Helgesen, P. Pieranski, A. T. Skjeltorp, *Phys. Rev. Lett.* **1990**, *64*, 1425.
[4] N. Casic, S. Schreiber, P. Tierno, W. Zimmermann, T. M. Fischer, *Europhys. Lett.* **2010**, *90*, 58001.
[5] a) M. E. Leunissen, H. R. Vutukuri, A. van Blaaderen, *Adv. Mater.* **2009**, *21*, 3116; b) N. Osterman, I. Poberaj, J. Dobnikar, D. Frenkel, P. Ziherl, D. Babić, *Phys. Rev. Lett.* **2009**, *103*, 228301.
[6] a) A. Snezhko, I. S. Aranson, *Nat. Mater.* **2011**, *10*, 698; b) B. A. Grzybowski, H. A. Stone, G. M. Whitesides, *Nature* **2000**, *405*, 1033.
[7] J. Dobnikar, A. Snezhko, A. Yethiraj, *Soft Matter* **2013**, *9*, 3693.
[8] a) S. C. Glotzer, M. J. Solomon, *Nat. Mater.* **2007**, *6*, 557; b) S. Jiang, Q. Chen, M. Tripathy, E. Luijten, K. S. Schweizer, S. Granick, *Adv. Mater.* **2010**, *22*, 1060.
[9] F. Caruso, *Colloids and Colloid Assemblies: Synthesis, Modification, Organization and Utilization of Colloid Particles*, Wiley-VCH, Weinheim, Germany **2004**.

[10] J. Yan, M. Bloom, S. C. Bae, E. Luijten, S. Granick, *Nature* **2012**, *491*, 578.
[11] a) I. Sinn, P. Kinnunen, S. N. Pei, R. Clarke, B. H. McNaughton, R. Kopelman, *Appl. Phys. Lett.* **2011**, *98*, 024101; b) S.-N. Yin, C.-F. Wang, Z.-Y. Yu, J. Wang, S.-S. Liu, S. Chen, *Adv. Mater.* **2011**, *23*, 2915; c) F. Liang, C. Zhang, Z. Yang, *Adv. Mater.* **2014**, *26*, 6944; d) R. M. Erb, N. J. Jenness, R. L. Clark, B. B. Yellen, *Adv. Mater.* **2009**, *21*, 4825.
[12] J. Yan, K. Chaudhary, S. C. Bae, J. A. Lewis, S. Granick, *Nat. Commun.* **2013**, *4*, 1516.
[13] a) M. Albrecht, G. H. Hu, I. L. Guhr, T. C. Ulbrich, J. Boneberg, P. Leiderer, G. Schatz, *Nat. Mater.* **2005**, *4*, 203; b) S. K. Smoukov, S. Gangwal, M. Marquez, O. D. Velev, *Soft Matter* **2009**, *5*, 1285; c) B. Ren, A. Ruditskiy, J. H. Song, I. Kretzschmar, *Langmuir* **2012**, *28*, 1149.
[14] T. C. Ulbrich, D. Makarov, G. Hu, I. L. Guhr, D. Suess, T. Schrefl, M. Albrecht, *Phys. Rev. Lett.* **2006**, *96*, 077202.
[15] L. Baraban, R. Streubel, D. Makarov, L. Han, D. Karnaushenko, O. G. Schmidt, G. Cuniberti, *ACS Nano* **2012**, *7*, 1360.
[16] Q. Chen, E. Diesel, J. Whitmer, S. C. Bae, E. Luijten, S. Granick, *J. Am. Chem. Soc.* **2011**, *133*, 7725.
[17] S. Kantorovich, R. Weeber, J. J. Cerda, C. Holm, *Soft Matter* **2011**, *7*, 5217.
[18] C. A. Neugebauer, *Phys. Rev.* **1959**, *116*, 1441.
[19] J. N. Israelachvili, *Intermolecular and Surface Forces*, Academic Press, London, UK **1991**.
[20] a) S. Jäger, S. H. L. Klapp, *Soft Matter* **2011**, *7*, 6606; b) J. Yan, S. C. Bae, S. Granick, *Soft Matter* DOI: 10.1039/C4SM01962H.
[21] K. Drescher, K. C. Leptos, I. Tuval, T. Ishikawa, T. J. Pedley, R. E. Goldstein, *Phys. Rev. Lett.* **2009**, *102*, 168101.
[22] P. Tierno, R. Muruganathan, T. M. Fischer, *Phys. Rev. Lett.* **2007**, *98*, 028301.
[23] A. P. Hynninen, M. Dijkstra, *Phys. Rev. Lett.* **2005**, *94*, 138303.
[24] N. Yanai, M. Sindoro, J. Yan, S. Granick, *J. Am. Chem. Soc.* **2012**, *135*, 34.
[25] S. H. Lee, Y. Song, I. D. Hosein, C. M. Liddell, *J. Mater. Chem.* **2009**, *19*, 350.
[26] a) O. Guell, F. Sagues, P. Tierno, *Adv. Mater.* **2011**, *23*, 3674; b) S. Sacanna, M. Korpics, K. Rodriguez, L. Colón-Meléndez, S.-H. Kim, D. J. Pine, G.-R. Yi, *Nat. Commun.* **2013**, *4*, 1688.
[27] C. Park, T. Lee, Y. Xia, T. J. Shin, J. Myoung, U. Jeong, *Adv. Mater.* **2014**, *26*, 4633.
[28] L. Hong, S. Jiang, S. Granick, *Langmuir* **2006**, *22*, 9495.
[29] a) M. B. Bannwarth, S. W. Kazer, S. Ulrich, G. Glasser, D. Crespy, K. Landfester. *Angew. Chem. Int. Ed.* **2013**, *52*, 10107; b) H. R. Vutukuri, J. Stiefelhagen, T. Vissers, A. Imhof, A. van Blaaderen, *Adv. Mater.* **2012**, *24*, 412.
[30] a) R. M. Erb, R. Libanori, N. Rothfuchs, A. R. Studart, *Science* **2012**, *335*, 199; b) J. Kim, S. E. Chung, S.-E. Choi, H. Lee, J. Kim, S. Kwon, *Nat. Mater.* **2011**, *10*, 747.
[31] V. Sharma, Q. Yan, C. C. Wong, W. C. Carter, Y.-M. Chiang, *J. Colloid Interface Sci.* **2009**, *333*, 230.